Figure 1.15: *Electron number* of a 0.5 TeV (green), of a 1 TeV (red) and a 3 TeV (blue) shower vs *depth* in units of radiation lengths.

case of electromagnetic showers solutions **exist** for the cascade equations which assume several approximations.

The **mean free path length** of an electron (distance at which the 1/e part of the electrons did not interact) is called the **radiation length** λ and has the size of $\lambda = 36.2 \frac{g}{cm^2}$. This quantity has to be divided by the density of the air to get the unit of a length (at sea level $\rho = 0.0011 \frac{g}{cm^3}$ it equates to approximately 350 m). For the following discussion four parameters are introduced:

- The **depth T** along the shower axis in radiation lengths λ..

- The **shower age** $s = 3/(1 + 2 * (y/T))$, which ranges from 0 to 2. The shower maximum is found at s=1.

- The **critical energy** $E_c = 80$ MeV, where the energy loss through ionization, equals the energy loss through particle multiplication.

- And a **variable** $y = \ln(E/E_c)$, where E is the energy of the initial gamma photon.

The approximate longitudinal electron number then becomes [Gai90]:

$$N_e(s) = \frac{0.31}{\sqrt{y}} e^{T(1 - 1.5 * \ln s)} \tag{1.24}$$

The **electron number** vs **depth** for a 3 TeV, a 1 TeV and a 500 GeV shower is plotted in Fig. 1.15.

By introducing a very simple exponential atmospheric model (neglecting temperature changes), one obtains an approximate shower shape as a function of height. The following equation relates the depth T (in radiation lengths) with the height H (in m):

$$T = \frac{X_0}{\lambda \cos \vartheta} e^{-\frac{H}{H_0}} \tag{1.25}$$

Where $X_0 = 1013 \frac{g}{cm^2}$ is the column height of air at ground, $H_0 = 8400$ m is the height at which the atmospheric pressure reduced to 1/e from the one at ground and $\vartheta = 0$ is the inclination angle of the shower axis.

The resulting plot in Fig. 1.16 shows a 3 TeV, a 1 TeV and a 500 GeV shower with respect to height according to the simple model described above. The shower maximum for a 1 TeV shower can be seen at approximately 9500 m. The shower maximum for showers with higher energy **reaches deeper** into the atmosphere.
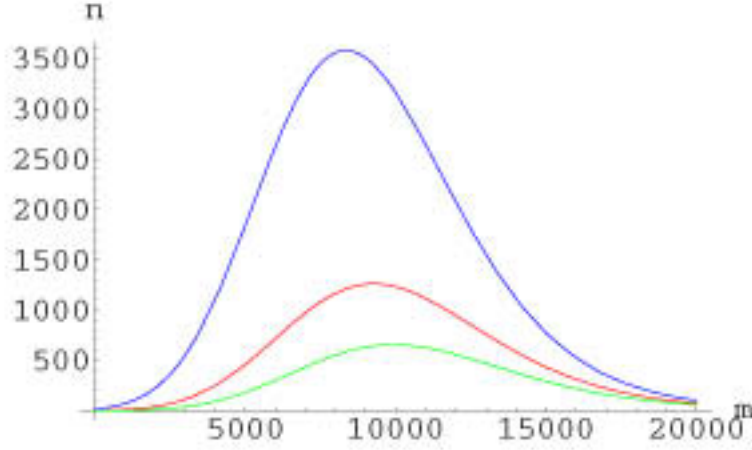
Figure 1.16: **Electron number** of a 0.5 TeV (green), of a 1 TeV (red) and a 3 TeV (blue) shower shower vs the **height** in m counted from ground. For higher energies the shower maximum **reaches deeper** into the atmosphere.

In order to understand the **asymmetric shape** of shower images seen by the camera, we analyze the **electron density** seen under an observation angle by the telescope (the Cherenkov image itself is far more complicated and will not be treated here). The transformation from the height coordinate to the viewing angle coordinate involves a **tangent** of that angle. This results in a **very asymmetric** shower image. Fig. 1.17 shows the same three showers developing at an impact parameter of **90 m**. Here it can be seen clearly that the shower image in the telescope camera is very asymmetric. The shower maximum moves to larger **distances** for in the camera for higher energies.

The camera of the CT1 telescope has an opening angle of approximately **1.4 degrees**. Comparing this with our image, it can be concluded that the recorded camera image will be **truncated**. For these reasons, two new image parameters have been introduced, as will be explained in detail in a later chapter. They are: an **asymmetry parameter,** and a **leakage parameter**, which describes the **degree of truncation** of the shower image due to a too small camera. The latter parameter will be used for energy estimation purposes.

There also exists an analytical solution for the **lateral width** of the shower. Unfortunately it is only valid for $1 \leq s \leq 1.4$ and is therefore **not very useful** for developing an analytical model for the shape of γ-showers. (Such a model might be useful for γ/hadron separation using log-likelihood techniques). It is the so-called **NKG-formula** displayed in Fig. 1.18:

$$x f(x) = K \, x^{s-1} \, (1+x)^{s-4.5} \tag{1.26}$$

where K is a normalization constant and

$$x = r/r_M \tag{1.27}$$

is the radial distance from the shower core in units of **Moliere radii**

$$r_M \approx 9.3 \frac{g}{cm^2}$$

The following expression defines the normalization constant K in Equ. 1.26:

$$2\pi \int_0^\infty x f(x) \, dx = 1 \tag{1.28}$$

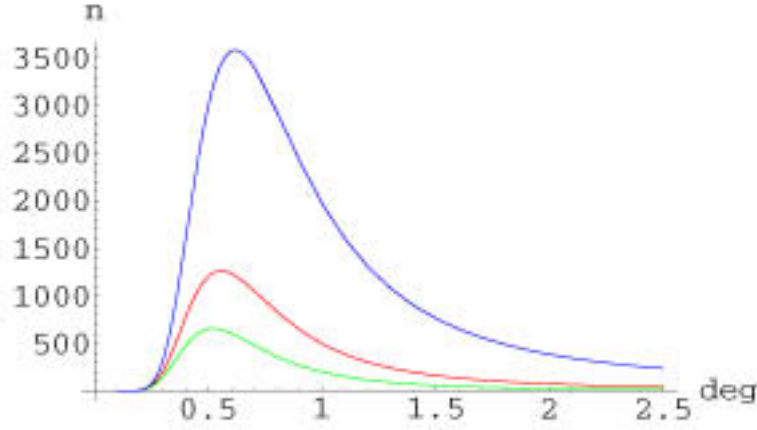Finally, the **lateral electron density** $\rho_N (r, T)$ becomes

Figure 1.17: *Electron number* of a 0.5 TeV (green), of a 1 TeV (red) and a 3 TeV (blue) shower vs the *viewing angle* from ground in degrees. For higher energies the shower maximum is found at *larger distances* in the camera.
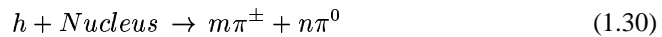
$$\rho_N\left(r, T\right) = \frac{N_e\left(T\right)}{r_M^2} f\left(x\right) \tag{1.29}$$

As a result, it can be stated that the *lateral spread increases* with the *shower age*. From the view of the camera the image develops from the center (if the center of the camera points to the source) to *bigger* viewing angles while the lateral spread continuously *increases*.

Hadronic showers are more complicated than electromagnetic ones and the cascade equations cannot be solved analytically. Usually *Monte Carlo simulations* are needed to understand the difference between electromagnetic cascades and hadronic cascades.

1.4.2   Hadronic cascades

A hadronic shower has *three* components, *a hadronic*, *an electromagnetic* and *a muonic* one. The shower develops as follows: A high energy hadron interacts with the nucleus of an atom in the air and produces mainly pions (and a few kaons).

$$h + Nucleus \rightarrow m\pi^\pm + n\pi^0 \tag{1.30}$$

The shower consists of a hadronic high energy core that continuously feeds the electromagnetic part because the π^0 instantly decay into two photons.

$$\pi^0 \rightarrow \gamma + \gamma \tag{1.31}$$

Each high energy photon emerging from the *hadronic core* creates an *electromagnetic sub-shower*. Lower energy charged K's and π's feed the *muonic component* by decaying into muons and neutrinos. At each hadronic interaction, *approximately one third* of the energy goes into the *electromagnetic component*. Since the hadrons usually re-interact, a large part of the initial energy finally ends up in the electromagnetic part and is dissipated through ionization losses and Cherenkov radiation. The most numerous particles in a hadronic shower are therefore positrons and electrons. It should be noted that in a hadronic shower a *sizeable fraction* of the energy is transported away by invisible neutrinos and muons and so that *only a fraction* of the initial energy is *deposited* in the atmosphere. Therefore hadronic showers produce *less* Cherenkov light than their electromagnetic counterparts.
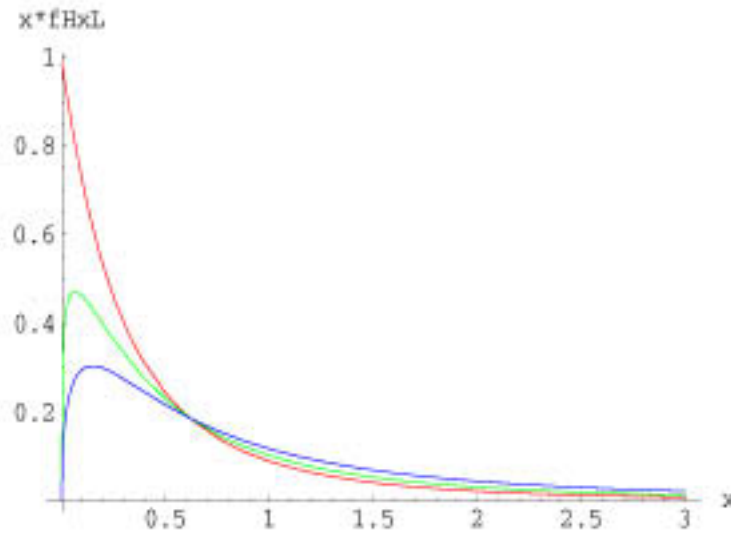
Figure 1.18: The function $xf(x)$ with correct normalization demonstrates the lateral electron distribution for s=1.0 (red), s=1.2 (green), s=1.4 (blue). The lateral distribution gets **wider** with shower age due to **multiple scattering**.

A Cherenkov telescope sees the Cherenkov radiation basically only from electrons and positrons because a) they are more likely to be **above threshold** of Cherenkov light production and b) they form the **overwhelming** fraction of particles in a shower. The image of an hadronic shower seen by such a telescope is wider and larger and has much **larger fluctuations** than that of a pure electromagnetic shower (see Fig. 1.14). The fluctuations are larger because the hadronic radiation length is almost double the size of the electromagnetic radiation length: $\lambda_h = 70 \frac{g}{cm^2}$. The **lateral spread** of the hadronic shower is mainly caused by the **transverse momentum** of the secondary hadrons after a hadronic interaction while in the case of electromagnetic showers the lateral spread is a function of **multiple scattering** resulting in a much slimmer shower.

Since one is interested only in gamma ray induced showers, the hadronic showers must be **separated** from the electromagnetic ones. This difference in the **geometrical** image structure, and to a certain extent the **time** structure, can be used to distinguish between the gamma induced events and the hadronic background, provided the instrument has sufficient resolution (e.g. a finely pixelized camera and sub-nanosecond time resolution).

It should be noted that an incoming high energy γ-photon (or a γ in the shower) can develop secondary hadrons with low probability (1%) via photoproduction which initiate a hadronic shower. Such showers, induced by a γ-photon, cannot be distinguished from a normal hadronic shower and therefore add to the background. However, most will be eliminated by selection cuts.

Below 100 GeV there exists a small but **non-negligible contribution of electrons** in the primary CR flux. These electrons initiate electromagnetic showers as primary γ's and are therefore indistinguishable from γ induced showers and so form a non-reducible background. However, like all the other charged CR, they are **isotropically distributed**. It is therefore essential to achieve a good angular resolution to reduce the e^- background in the case of point source searches.

All the structure of extended air showers can be seen through the Cherenkov light emitted by the particles (with $\beta \geq \beta_c$) in the shower. Cherenkov telescopes are especially sensitive to the **directionality** of the Cherenkov light. This is an important difference to air **fluorescence** experiments.

1.4.3   Cherenkov light production

A highly relativistic particle emits Cherenkov light during its travel through the atmosphere [Jel58, Lon1/92]. Cherenkov light is always produced when the particle velocity is **faster then the velocity of light** in the air ($\beta \geq \beta_c$). The condition for Cherenkov light production therefore is:

$$\frac{c}{n\left(\rho,\omega\right)} < v = \beta c = (1 - \frac{1}{\gamma^2})c \tag{1.32}$$

where $n\left(\rho,\omega\right)$ is the refraction index of the atmosphere which **depends** on the **density of the air** and the **wavelength**, β is the velocity of the particle in units of c and γ is the relativistic Lorentz-factor. The condition above also **limits the spectral range** of the Cherenkov-light since the refraction index of the air depends on the wavelength. The Cherenkov light is radiated in a light cone of opening angle

$$cos\left(\theta\right) = \frac{1}{\beta n\left(\rho,\omega\right)} \tag{1.33}$$

The maximum opening angle **increases** as the particle enters deeper in the atmosphere due to the increasing air density. This is illustrated in Fig. 19.The Energy radiated per unit length and unit frequency is [Lon1/92]:

$$\frac{dE}{dl} = \frac{e^2\omega}{4\pi\varepsilon_0 c^3}\left(1 - \frac{c^2}{n^2\left(\rho,\omega\right)\nu^2}\right) \tag{1.34}$$

The Cherenkov light seen from the ground is the **superposition** of all the light emitted in cones by all the electrons and positrons integrated over the whole shower development.

In order to determine the total light distribution on the ground, the **lateral spread** of the electrons and more importantly, the **angular distribution** $q\left(\beta,h\right)$ of the **propagation direction** of the electrons, which defines the **direction of emission** of the Cherenkov cone, has to be taken into account. Fig. 19 shows the distribution of Cherenkov light emitted by a 1 TeV shower.

.1   The principle of Cherenkov imaging telescopes

Air showers develop practically with the speed of light, resulting in very short Cherenkov light flashes. Typical numbers for the arrival time of Cherenkov photons are 2-4 ns for an electromagnetic shower. Hadronic showers have a wider time spread (10 ns - 15 ns) due to the development of many sub showers. Fig. 20 shows the Cherenkov photon density on ground for different CR particles. The **photon density** for electromagnetic showers on the ground **scales to first order with the energy** (for E > few GeV; the light output is used as the main energy estimator) while for protons this relation does not hold below 1 TeV. Reasonable mirror areas are needed to collect a sufficient amount of light for detection.

For example, for a **1 TeV** electromagnetic shower **only about** 100 photons/m^2 arrive the ground in the main impact parameter region of a radius of about 120 m, within the wavelength region of 300 nm (the ozone cutoff) to 600 nm (the sensitivity limit of the PMT). Assuming a collection mirror **area of** $\sim 10\,m^2$ for the CT1 telescope and taking into account losses in the optics, **only about 800 photons** will arrive to the (whole) camera during a few nanoseconds. During this time also light from the **night sky** (NSB) is continuously being collected by the mirror. On the Roque de los Muchachos in La Palma at 2300 m (the location of the CT1 telescope, the NSB accounts for approximately $4.3\ 10^{12}\ \frac{photons}{s\,m^2\,sr}$ [Sch00]. For $\sim 10\,m^2$ and a pixel diameter of $0.25°$ (corresponding to the CT1 telescope) this results in approximately **0.6 photons per ns and per pixel.** This number depends strongly on the sky area and weather conditions and can easily change by a factor of 2 or
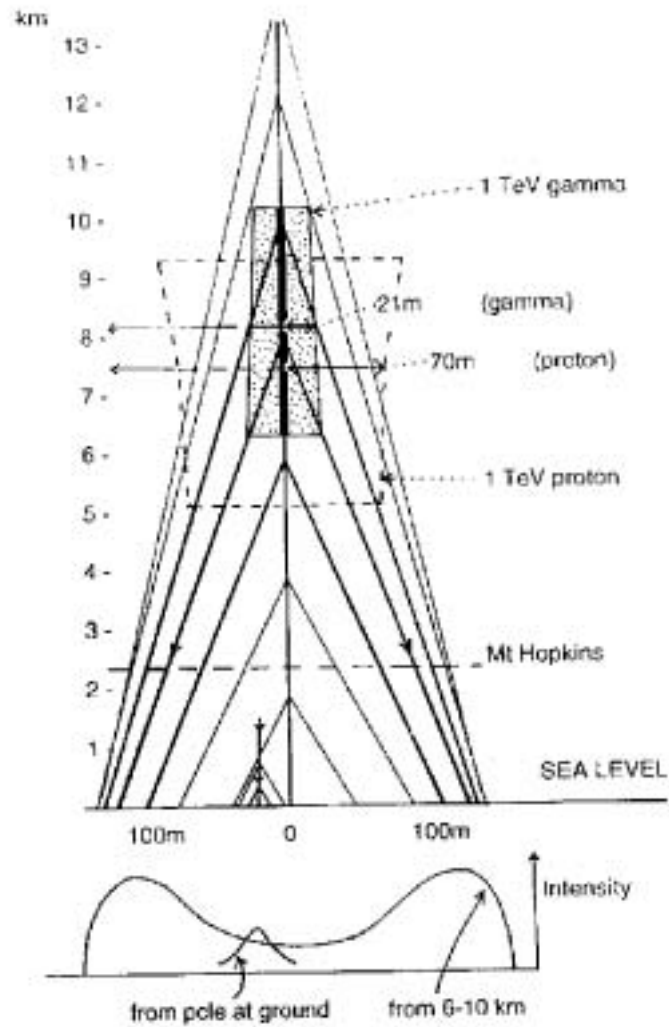
Figure 19: This figure sketches the Cherenkov light production of a 1 TeV photon. It illustrates how the opening angle increases with the density of the air. Most of the light is emitted between a height of 10 km and 6 km. (taken from [Hil96])
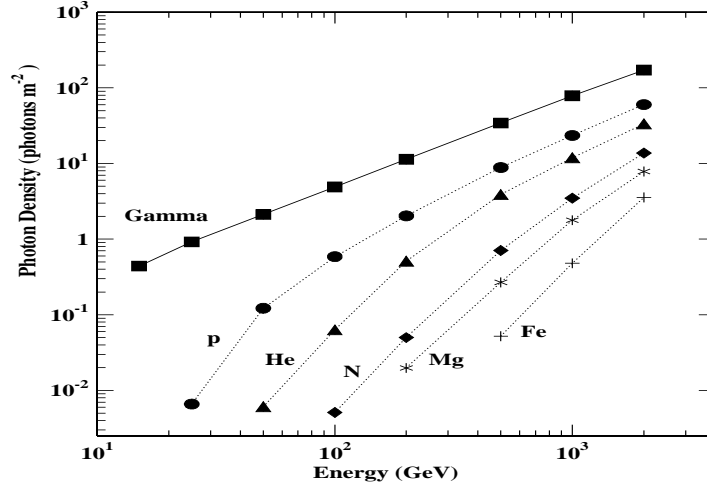
Figure 20: Cherenkov photon density (300 nm-600 nm) of different cosmic ray particles at 2000 m averaged over $50000\,m^2$ collection area (impact parameter $<\,125\,m$), taken from [Ose01]

more in time scales of 20 minutes, depending on the humidity of the air. During moon light, the night sky background can be up to **two orders of magnitude higher**.

The **brevity** of the light flash defines the properties that a camera must have: **Single photon counting capability**, **ultra short recording time** of a few nano seconds, and the ability to **withstand** a rather high continuous photon background rate. This can be achieved with a camera consisting of pixels of photomultipliers, which are run at a sufficiently low gain to avoid damage by high currents, but still high enough to resolve at least a few photon pulses.

The size of the pixels should be smaller **than 0.3°** to at least be able to resolve the lateral spread (To see the fluctuations in the lateral distribution, the pixel diameter should ideally be below 0.1°) because the main advantage of an imaging telescope is to be able to distinguish between background (hadronic showers) and signal (gammas showers) **by seeing differences** in the image of the showers.

To bolster the above mentioned numbers lets give a numerical example: For a 1 TeV gamma shower the maximum is located at about an altitude of 10 km and the interaction length is about 1 km at that air density. Assuming the telescope is located at 2.2 km el-evation, then the interaction length corresponds to $\sim\,0.1°$ viewing angle in longitudinal direction for an impact parameter of $p = 100$ m. According to the NKG formula Equ. 1.26, the lateral spread for such a shower is half width half maximum d=65 m at s=1 (shower maximum) at that altitude of 10 km. A movement of 64 m perpendicular to the center-core connection line at the same impact parameter results in approximately 0.3° which corresponds to one CT1-pixel in lateral direction in the camera (see Fig. 1.14).

In the following sections I will give an overview of the HEGRA experiment and how the CT1 telescope, a major prototype for all Cherenkov telescopes has been implemented.

.2   The HEGRA experiment: An overview

The original HEGRA experiment (see Fig. 21) was proposed by the institute of physics the Universität Kiel and was built as a small scintillator array in 1988 on the Canary Island La Palma (28.75° N, 17.89° W). Gradually more institutes joined and the detector was enlarged. At present, the HEGRA collaboration consists of seven institutes: Universität Hamburg, Max-Planck-Insitut für Physik in Munich, Max-Planck-Institut für Kernphysik
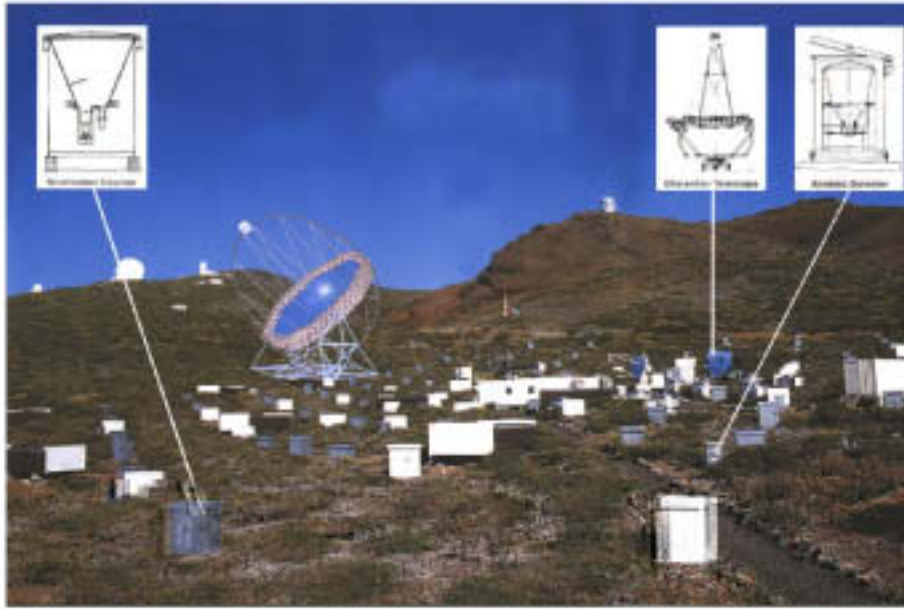
Figure 21: The HEGRA experimental site 1998. A collage shows the new MAGIC telescope which is currently under construction. On the right one can see the CT1 telescope which has been used to record the data for this thesis.

in Heidelberg, Universität Kiel, University of Madrid, Universität Wuppertal and the Yerevan Physics Institut in Armenia. The HEGRA experiment is located at the site of the **Observatorio del Roque de los Muchachos** at about 2200 m above sea level. In its 1997 setup, the experiment consisted of 17 Geiger counters, 244 scintillator counters, 77 wide angle Cherenkov counters and 6 Cherenkov telescopes. In the past year parts of the experiment have terminated and have been removed. At present only six Cherenkov telescopes are in use. Five of them are operated together in stereo mode in the so-called CT-system. The oldest telescope and original prototype of the experiment, is run in a stand-alone mode. This is the CT1 telescope. Only data from the CT1 telescope has been used for this thesis.

The CT1 telescope was installed 1992. In the beginning it had $5\,m^2$ of mirror area and a camera of 37 pixels with $\sim\ 3°$ field of view (FOV) [Mir94]. In December 1994 the camera was replaced by a higher resolution camera with **127 pixels** and a $\sim\ 3°$ FOV [Rau95]. CT1 was operated in this configuration until November 1997, at which time it was upgraded to $\sim\ 10\,m^2$ of mirror collection area made from aluminum mirrors. This represents the current setup used for this thesis. In this configuration **it has a threshold of approximately 750 GeV**.

The second HEGRA Cherenkov telescope, CT2, was installed in 1993. In contrast to CT1, which has an equatorial mount, CT2 uses an alt-azimuth mount and is equipped with $8.5\,m^2$ mirror area. In the beginning CT2 had a camera with only 61 pixels, but it was upgraded in 1998 to a high resolution camera of 271 pixels and $4.9°$ field of view. CT2 was also operated in stand-alone mode until 1998, when it was included in the CT-system. In 1997 it had a threshold energy of approximately 1 TeV.

The Cherenkov telescope system, called **CT-system**, consists of a set of four telescopes (namely CT2 to CT5). Together they are **operated in stereo mode**. This means that all of the telescopes watch the same object and simultaneously record the same air shower. In this way the impact parameter and therefore the energy can be reconstructed much more precisely. The advantage of having several images of the same shower leads to a much **improved gamma/hadron separation**. It is possible to obtain an **almost perfectly clean data set of gamma showers** when operating in a ≥ 3-fold telescope coincidence. The first

telescope of the CT system, CT3 was installed in 1995. CT4, CT5 and CT6 followed and were fully constructed end of 1996. All of these telescopes have a segmented mirror of $8.5\,m^2$ and a high resolution camera of 271 pixels and 4.9 ° FOV. The energy threshold of the system is 500 GeV.

.3   The HEGRA CT1 telescope

The CT1 telescope has always been referred to as the '***prototype telescope***' because it was the first telescope of the HEGRA collaboration (see fig. 22) . It was constructed in order to gain experience with these types of telescopes and to see if Cherenkov telescopes, in general, are able to record weak astrophysical signals with sufficient signal to noise ratio to observe astronomical objects and to perform real physics. It has been one of the first imaging Cherenkov telescopes in the world. In contrast to most Cherenkov telescopes it has an equatorial mount instead of an alt-azimuth mount. This has both advantages and disadvantages. ***The advantages are***

- The operation of an equatorial mounted telescope is simpler because ***only one axis and one motor*** are necessary to rotate with ***constant speed*** in order to counteract the rotation of the earth.

- The ***coordinate system*** of the camera ***does not rotate*** with respect to the coordinate system of the sky. All of the bright stars in the field of view of the camera stay in the same position. This simplifies the Monte Carlo simulation and the analysis, as described later in chapter A.

The disadvantages are

- The axis of the telescope is ***never aligned perfectly*** to the earth's rotation axis and therefore the data needs a ***pointing correction***[3] later on.

- The construction ***requires a heavy counter weight*** for the mirror dish. This sets limitations on the accessible angular range. The use of counterweights requires a very stable and therefore ***expensive construction***.

Nowadays Cherenkov telescopes are constructed only with ***alt-azimuth mounts***.

.3.1   Technical details

In the present setup CT1 is equipped with segmented hexagonal aluminum mirrors of 490 cm focal length. A so-called Davis-Cotton configuration has been chosen in order to obtain an optimal shape of the reflector with respect to ***best images*** (least distortion). The total mirror area is $\sim 10\,m^2$ with a reflectivity better than 80%.

The camera consists of 127 10-stage EMI-9083A PMTs connected to hexagonal light concentrators, so-called Winston cones' which accept only light coming from a limited angular range in the direction to the mirrors in order to block stray-light and background light emerging from the side. The PMTs are operated at medium gain with only 8 stages coupled to fast preamplifiers to compensate for the reduced gain. This is done to avoid high anode currents generated by the light of the night sky (NSB) and bright stars in the field of view.

During dark nights (without moon light), the ***NSB*** gives approximately ***0.6 photon/(ns*pixel).*** This corresponds to approximately ***0.3 photoelectron/pixel*** (integrated over a gate length

---

[3]The word 'mispointing' is used in the sense that the center of the camera does not coincide exactly with the coordinates of the object to which the telescope is pointing to. A 'pointing correction' corrects the data for slight misalignments.

Figure 22: An image of the CT1 telescope in present state in La Palma on the Roque de los Muchachos. The data used in this thesis has been recorded with it.

of around 30 ns). This number increases by a factor of two with different weather conditions and by a **factor of up to 20** during moon light hours. In the latter case the high voltage (HV) of the PMTs is reduced to keep the current in an acceptable range. The diameter of one pixel is $0.25°$ ($\hat{=}$ 21mm). This is barely sufficient to resolve the lateral distribution of air showers. The camera is the most expensive part of an air Cherenkov telescope. Therefore one has to make compromises in the choice of the pixel-diameter and FOV. The total FOV is $3°$. The maximum quantum efficiency (QE) of the PMT is 26% at 375 nm. The tracking error of the equatorial mount is $0.03°$ and the pointing error $< 0.15°$. The output of the pre-amplifiers is transfered to the counting container via coaxial cables.

.3.2 The trigger of CT1

The telescope triggers on incoming air-showers on the condition that within 6 ns (8-2 ns minimum overlap) two neighboring pixels out of any 127 show a signal higher than 50 mV, which corresponds to a superposition of approximately 13 photoelectrons in the PMTs. The trigger signal opens the gate of 127 charge sensitive (LeCroy) ADCs and initiates a readout signal. For each triggered event the direction of the telescope (via shaft encoder values) and a time stamp (via a rubidium clock) are recorded. The **trigger rate** depends on the **HV** of the PMTs, the **zenith angle** of the telescope and weather **conditions** on the mountain. The camera and the readout electronics are described in more detail in [Rau95]. For zenith angle $\vartheta = 0$ the trigger rate is approximately 5-8 Hz and the **energy threshold is about 750 GeV.**

.4 The All Sky monitor of the RXTE satellite

Sources that emit high energy (HE) γ-radiation normally also show strong keV-MeV γ-emission. These measurements have been carried out by satellite borne instruments be-
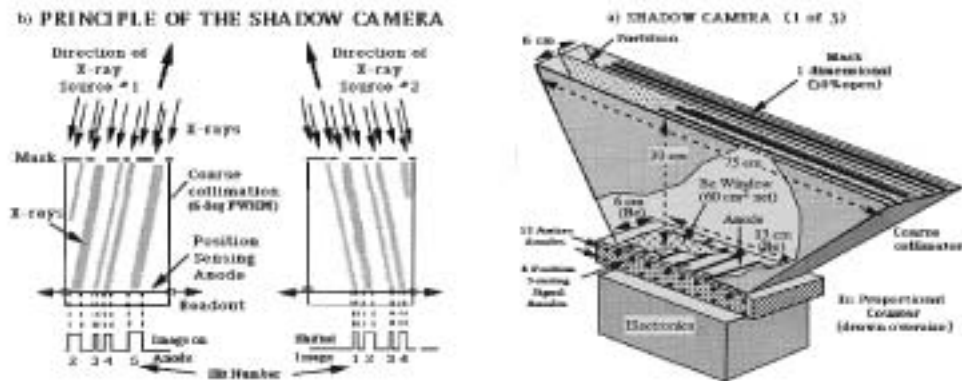
Figure 23: a) Principle of the Shadow Camera b) Schematic diagram of the Scanning Shadow Camera of the all sky monitor of the RXTE satellite.

cause the earth's atmosphere is an efficient shield. In chapter B, concerning the analysis of Mkn 421 observations, I will make use of x-ray observation data from the **RXTE satellite**. Here I give a brief overview of this instrument.

The RXTE satellite [Bra93], launched on December 30, 1995, was designed to probe cosmic X-ray sources on variability time scales in the range of milliseconds to years. On board of the satellite three experiments have been installed which span an energy range of 2 keV to 250 keV. They are:

- **Proportional Counter Array** (**PCA**): The PCA consists of five xenon gas proportional counters with a collection area of about 6200 cm^2. The PCA is sensitive to X-rays in the energy range from 2 keV to 60 keV and can measure short term variability down to the microsecond level.

- **High Energy X-ray Timing Experiment** (**HEXTE**): HEXTE consists of two independent clusters of four NaI/CsI phoswich scintillation detectors. The energy range is 15-250 keV and the time resolution is again a few microseconds.

- **All Sky Monitor** (**ASM**): The ASM is the detector whose data has been used in this thesis. The ASM consists of three Scanning Shadow Cameras (SSCs) and covers an **energy range from 2 to 12 keV**. The SSC has a slit mask at the entrance (see fig. 23), that produces a characteristic shadow pattern in the Position Sensitive Proportional Counters (PSPC) which are filled with Xenon. The idea is that each source in the sky produces such a pattern in the detector and that the pattern of all sources superpose. Deconvoluting the image delivers the intensity and direction of the individual sources. The ASM scans 80 % of the sky every 1.5 h and is used to measure long-term variability (hours to months) of bright X-ray sources due to the rotation of the satellite. All three SSCs point in different directions of the sky. **The data is delivered in 90 second bins**.

For a more complete description of ASM and HXTE see [Lev96, Gru96].